Tectonophysics 546-547 (2012) 56–59

Contents lists available at SciVerse ScienceDirect

Tectonophysics

journal homepage: www.elsevier.com/locate/tecto

Material decoupling as a mechanism of aftershock generation

Chien-chih Chen [a,*], Jeen-Hwa Wang [b], Wen-Jeng Huang [a]

[a] Graduate Institute of Geophysics & Department of Earth Sciences, National Central University, Jhongli, Taoyuan 320, Taiwan
[b] Institute of Earth Sciences, Academia Sinica, Nangang, Taipei 115, Taiwan

ARTICLE INFO

Article history:
Received 16 June 2011
Received in revised form 4 April 2012
Accepted 22 April 2012
Available online 1 May 2012

Keywords:
Spring–block model
Omori–Utsu law
Aftershocks
Stiffness
Damage mechanics

ABSTRACT

Aftershocks following a large mainshock are characterized by clustering in space and time. The temporal decay in the number of aftershocks follows the empirical Omori–Utsu law. Aftershocks are regarded as delayed responses to stress changes induced by the mainshock; therefore, conventional wisdom dictates that the mechanical Maxwell or Kelvin element must be taken into account when modeling aftershock generation. We propose a novel mechanism of aftershock generation by evaluating changes in the stiffness ratio (or stiffness between two blocks) of a dynamical one-dimensional spring–block model. Simulations reveal the existence of spatiotemporal event clustering (i.e., aftershocks) associated with a preceding large event (i.e., the mainshock). In addition, the empirical Omori–Utsu law, with $p \sim 0.8$, can hold for many sequences of numerical aftershocks produced in our model. Therefore, we suggest that changes in the stiffness or strength of materials play an important role in aftershock generation.

© 2012 Elsevier B.V. All rights reserved.

1. Introduction

Aftershocks occur after most large earthquakes and make up the majority of earthquake catalogs. However, the mechanisms that generate aftershocks are still under debate (Scholz, 1990). Aftershocks are conventionally considered to be the byproduct of stress alterations in the crust induced by mainshocks through time-dependent processes such as pore-fluid flow, viscous relaxation of the lower crust and upper mantle, and afterslip. Viscoelastic relaxation, which is a common mechanism for generating aftershocks, can be mechanically represented by a combination of springs and dashpots (Hainzl et al., 2000; Scholz, 1990; Wang et al., 2009).

Changes in the elastic modulus (in terms of stress) of materials with slip or strain are widely observed in experimental stress–strain curves (Fig. 1) and are dependent upon temperature (Atkinson, 1987; Scholz, 1990). Materials in the low-strain regime generally obey Hooke's law; therefore, stress is proportional to strain with the proportionality constant which is defined as Young's modulus of elasticity. However, as strain becomes larger than a threshold value, the stress–strain relationships for many materials eventually deviate from the linear portion of the curve. This relationship results in anelastic (i.e., plastic, ductile, and viscoelastic) behavior. The general conceptual picture is that, microcracking in a material exposed to a high-strain regime can weaken the material and cause it to deviate from the linear elasticity. A continuum approach to the damaging process thus introduces an *effective* Young modulus, which is not a constant and depends on the so-called damage variable (Shcherbakov and Turcotte, 2004; Turcotte et al., 2003). The mean-field approximation of the microscopic fiber-bundle model suggests that the effective Young's modulus decreases from its intact value to zero when a brittle material fails.

In this study, we apply a one-dimensional (1-D) N-degree-of-freedom dynamical spring–block model (Burridge and Knopoff, 1967; Chen and Wang, 2010; Wang, 1995; Wang, 1996) with varying strengths in elastic modulus to simulate the spatiotemporal distribution of earthquakes. Our simulations find the spatiotemporal event clustering (i.e., aftershocks) associated with a preceding large event (i.e., the mainshock). This study also discusses the temporal variation in numerical aftershocks.

2. 1-D spring–block model with changeable stiffness

The 1-D model consists of N blocks with equal mass, m, and springs with one block being linked by a coil spring of strength, K_C, to the neighboring blocks. Each block is also pulled by a leaf spring of strength, K_L, from a moving plate with a constant velocity, V_p. Each block is furthermore subjected to a frictional force with a static value, F_{Si} ($i = 1, \ldots, N$), at rest. The elastic force at each block exerted by the moving plate through the leaf spring gradually accumulates. Once the elastic force at a given block is greater than the static frictional force, the block will move, and the frictional force will drop from the static value to the dynamic value, F_{Di}, thus generating an event (Chen and Wang, 2010). One crucial parameter in the spring–block model is the stiffness ratio, S ($= K_C/K_L$). This ratio represents the level of conservation of energy in the system (Wang, 1995). Larger values for S demonstrate stronger coupling between two blocks than between the block and the moving plate, which results in smaller energy losses through the leaf spring and indicates a higher level of energy

* Corresponding author. Tel.: +886 3 422 7151x65653; fax: +886 3 422 2044.
E-mail address: chencc@earth.ncu.edu.tw (C. Chen).

0040-1951/$ – see front matter © 2012 Elsevier B.V. All rights reserved.
doi:10.1016/j.tecto.2012.04.016

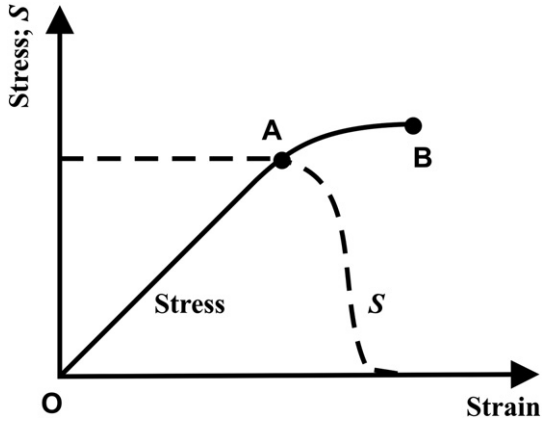

Fig. 1. Illustration of linear (O–A) and nonlinear (A–B) elastic behavior of a strained material. Microcrack density gradually increases, and the material starts to weaken after point A. Macrocracking is ready to occur at point B immediately before the material breakdown. The variations in stress and S are plotted with solid and dashed lines, respectively.

conservation in the system. Intuitively, S can be regarded as an indicator of the effective elastic modulus of the material. In this study, we explore the effect of a change in S on earthquake occurrences. Our proposition is that S is constant when the displacement of a block is smaller than a threshold, and S drops to zero when the displacement of a block reaches that threshold. The variation in S is schematically shown in Fig. 1 with a dashed line. S recovers to its initial value after the block arrests. It is notable that the variation in S is caused by a change in K_C rather than K_L and may be related to the change in state variables in the rate- and state-dependent friction law (Dieterich, 1994). Dieterich, 1994 had incorporated the spring stiffness of single spring–slider system in the multiple state representation of fault friction (Eq. (5) in Dieterich, 1994). Although he did not explicitly investigate the effect in seismicity of stiffness change, he argued that spring stiffness may be scaled to crack length (Eq. (A1) in Dieterich, 1994). His argument quite coincides with our motivation and the consequence is examined in this paper.

3. Spatiotemporal clustering and the Omori–Utsu law for numerical aftershocks

Fig. 2(a) shows an example of the space–time plot of 1000 simulated earthquakes. A red dot represents the block at which rupture was initiated, which is the hypocenter of the simulated event. The white vertical bar displays the 1-D spatial distribution along the vertical axis of all ruptured blocks during an event. The horizontal axis shows the sequential number of events, indicating the event occurrence order in time. Therefore, a bundle of white vertical bars (e.g., Clusters A and B) are successive earthquakes that occurred at neighboring blocks. In other words, we can see the sequences of simulated earthquakes with spatial clustering when S changes. Fig. 2(b) reveals the size-time plot of simulated earthquakes centered more or less at the occurrences of Clusters A and B. The size of an event is defined as the logarithmic value of the seismic energy of an event (Wang, 1995). Therefore, the size of an event is defined by the number of ruptured blocks (Chen and Wang, 2010). The frequency-size distribution of simulated earthquakes by this S-changeable model demonstrates the common power–law scaling for the usual spring–block models with constant S (Wang, 1994, 1995, 1996). Yet another significant feature in Fig. 2(b) is that some events associated with Clusters A and B occurred in a short time interval. For example, at least eight events for Cluster A and six for Cluster B occurred over a short time. These events occurred one by one with an interval of a unit of time in computation. Consequently, sequences of earthquakes with temporal clustering can be also generated in this S-changeable model.

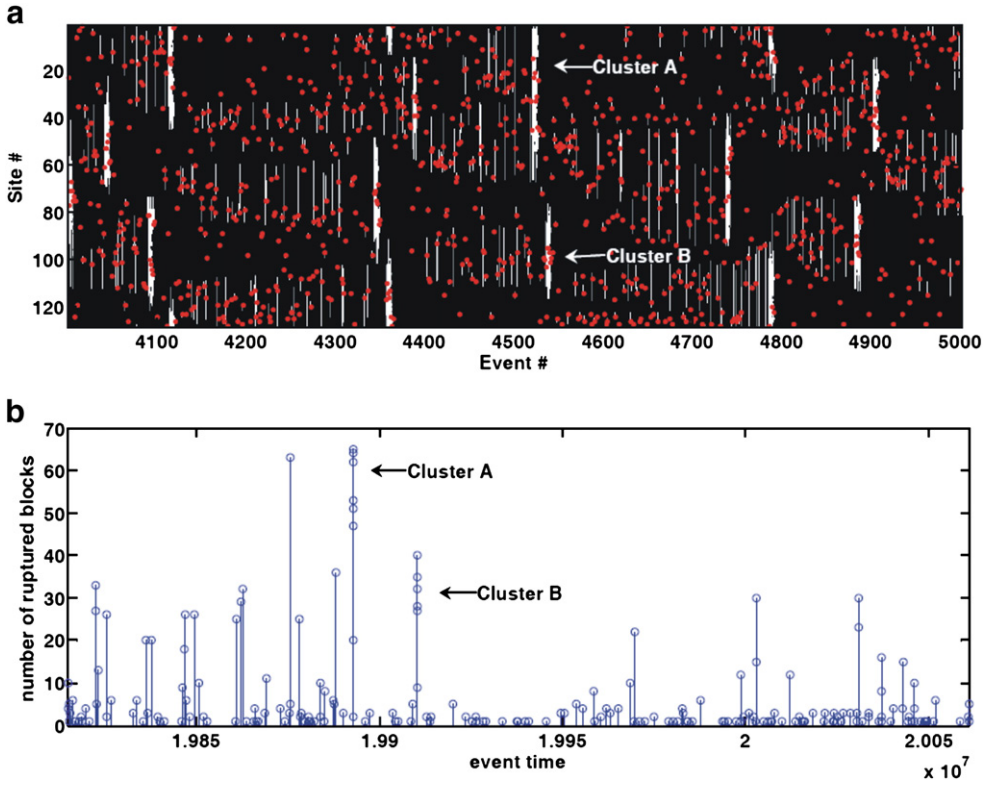

Fig. 2. (a) Space–time and (b) size–time plots of 1000 simulated earthquakes from Event #4001 through Event #5000 in the S-changeable spring–block model. The white vertical bar in (a) displays the 1-D spatial distribution along the vertical axis of all ruptured blocks during an event while the horizontal axis shows the sequential number of each event indicating the event occurrence order in time. The model shows an important feature of spatiotemporal clustering noted in real earthquakes.

Fig. 2 clearly shows that a large mainshock is often followed by the spatiotemporal clustering of aftershocks. These results point to an important question: can aftershocks simulated in the *S*-changeable model follow the empirical Omori–Utsu law (Omori, 1894; Utsu, 1961; Wang, 1994) obtained from natural aftershocks? To answer this question, the cumulative number of events in terms of time is displayed in Fig. 3. The average seismicity rate is ~62 events per 10,000 time units, which results in a linearly increasing trend when plotting a curve of cumulative event numbers. However, some bay-shaped increments are superimposed on the linear trend. These bay-shaped increments are evidently another manifestation of mainshock–aftershock temporal clustering. The cumulative number of aftershocks as a function of time is shown in Fig. 4. The total number of aftershocks in our simulations is generally less than 50 because the number, N, of blocks is only 128. Therefore, we used the integral form of the Omori–Utsu law instead of the differential one. The integral form of the Omori–Utsu law is $n(T)\equiv\int_0^T dn=\frac{k}{1-p}\left[(c+T)^{1-p}-c^{1-p}\right]$, where $n(T)$ is the cumulative number of aftershocks at time, T, after the mainshock. The parameters k and c are related to the aftershock productivity and the time offset of aftershocks, respectively, and the exponent p is associated with the decay rate of aftershocks (Omori, 1894; Utsu, 1961). The cumulative numbers of simulated aftershocks for the first bay-shaped increment displayed in Fig. 3 are shown with open circles in Fig. 4. In total, 27 aftershocks occurred in a time interval of ~6000 units in this example. The integral Omori–Utsu law inferred from the data points is depicted by a red solid curve with $k=0.70\,(\text{time units})^{-1}$, $c=2.22\times10^{-14}$ time units, and $p=0.74$. This curve fits the data points very well with a goodness-of-fit value of $R^2=0.89$. For real aftershocks, the observed p-value is typically close to 1.0 but falls mainly in a range from 0.5 to 1.5 (Scholz, 1990; Wang, 1994). From more than 200 sequences of simulated aftershocks produced using the present model, we obtained $p=0.78\pm0.39$. Therefore, the *S*-changeable spring–block model is able to generate aftershocks following the empirical Omori–Utsu law with a reasonable p-value when compared with real aftershocks.

4. Concluding remarks

Considering the spring–dashpot model in response to a stress σ, a dashpot with the viscous coefficient η relaxes at a rate of σ/η while a spring with stiffness K deforms at a rate of σ/K. The dashpot in a Maxwell or Kelvin element produces the viscous effect and delays the response to the exerted stress. In this study, we did not invoke a dashpot for stress

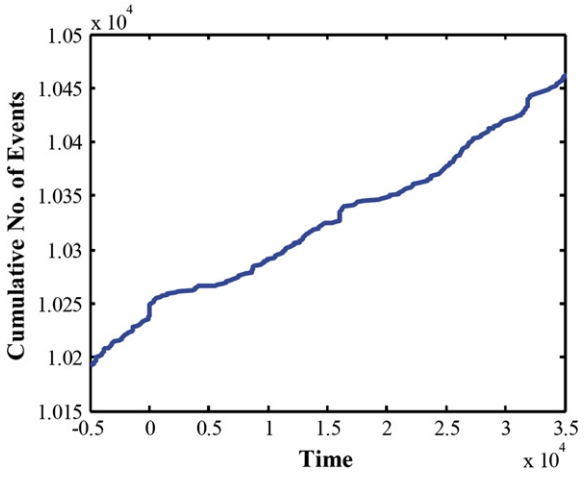

Fig. 3. Temporal variation in the cumulative number of simulated events. The average seismicity rate is ~62 events per 10,000 units of modeling time; therefore, the curve plotting the cumulative number of events follows a linearly increasing trend. Bay-shaped increments are superimposed on the linear trend. Time origin has been shifted to the first bay-shaped increment.

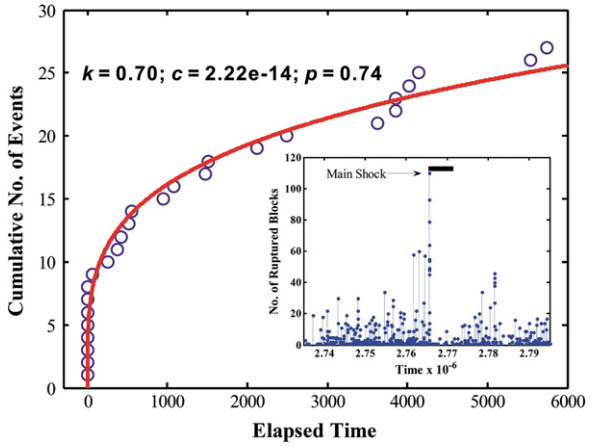

Fig. 4. Cumulative numbers of simulated aftershocks for the first bay-shaped increment in Fig. 3. The integral Omori–Utsu law fits these data well. The inset shows the size–time plot around this sequence of main shock and aftershocks, and the main shock is indicated by the arrow and aftershocks by horizontal bar.

relaxation but instead changed the stiffness of the spring–block model. Mechanically, both the viscous dashpot and the stiffness change represent a deviation from the initially linear relationship in the stress–strain curve (Fig. 1) and fulfill, in a general sense, the definition of anelasticity. In our simulations, zero stiffness is supposed to prevent energy transfer between two blocks during ruptures from a mainshock, and this effect should generate post-seismic slips and events possibly induced by *residual* energy after the mainshock. Note that we have simply defined mainshocks as the events with more blocks ruptured than others and no additional mechanism, e.g. the viscous dashpot, is included in the *S*-changeable spring–block model for producing aftershocks. In other words, our study is in favor of the view that an aftershock is nothing different from a mainshock except for slipped blocks less than a mainshock. The earthquake process, regardless of mainshocks, foreshocks and aftershocks, thus represents a process of self-organization and cooperative behavior of the entire system (Chen et al., 2006; Hainzl et al., 2000). Our simulations might then indicate that microcracking not only weakens the material strengths from a macroscopic viewpoint but also plays a crucial microscopic role by decoupling from neighbors a fault block which reaches a threshold of displacement. This decoupling effect, instead of the viscous effect, could be favored in the shallow crust under brittle conditions.

An important question remains: how can we verify the existence of decoupling? One possible way is through the "precise" measurement of post-seismic displacements. Post-seismic slip is conventionally explained by deformation due to viscoelastic relaxation in an exponential decay fashion (Brenguier et al., 2008; Hsu et al., 2006, 2009; Scholz, 1990). Based on the decoupling hypothesis, it is not necessary to have a smooth exponentially-decreasing post-seismic slip, as suggested by the viscoelasticity relaxation model (Brenguier et al., 2008). By contrast, some irregularities can be present in the post-seismic slip. The presence of irregularities in the observed post-seismic displacements (Hsu et al., 2006, 2009) could be evidence of the decoupling mechanism.

In summary, the effect of a change in stiffness ratio (or stiffness between two blocks) on seismicity of the spring–block model was studied. Simulation results show that the change in the stiffness ratio can produce spatiotemporal clustering of aftershocks that follow the Omori–Utsu law. Therefore, we argue that the change in stiffness (or strength) in the crust plays a crucial role in generating crustal aftershocks. Because the stiffness ratio in our simulations recovers from zero back to the initial value soon after the event ceases, an immediate implication can be therefore drawn from this study that fault healing occurs on a shorter time scale than aftershock generation (Marone et al., 1995; Scholz, 1990).

Acknowledgments

CCC is grateful for research support from the National Science Council (ROC) and the Department of Earth Sciences, National Central University (ROC). JHW was supported by the Academia Sinica. We are indebted to anonymous reviewers for their helpful comments.

References

Atkinson, B.K., 1987. Fracture Mechanics of Rock. Academic Press, New York.
Brenguier, F., Campillo, M., Hadziioannou, C., Shapiro, N.M., Nadeau, R.M., Larose, E., 2008. Postseismic relaxation along the San Andreas fault at Parkfield from continuous seismological observations. Science 321, 1478–1481.
Burridge, R., Knopoff, L., 1967. Model and theoretical seismicity. Bulletin of the Seismological Society of America 57, 341–371.
Chen, C.C., Wang, J.H., 2010. One-dimensional dynamical modeling of slip pulses. Tectonophysics 487, 100–104.
Chen, C.C., Rundle, J.B., Li, H.-C., Holliday, J.R., Turcotte, D.L., Tiampo, K.F., 2006. Critical point theory of earthquakes: observation of correlated and cooperative behavior on earthquake fault systems. Geophysical Research Letters 33, L18302, http://dx.doi.org/10.1029/2006GL027323.
Dieterich, J., 1994. A constitutive law for rate of earthquake production and its application to earthquake clustering. Journal of Geophysical Research 99, 2601–2618.
Hainzl, S., Zöller, G., Kurths, J., Zschau, J., 2000. Seismic quiescence as an indicator for large earthquakes in a system of self-organized criticality. Geophysical Research Letters 27, http://dx.doi.org/10.1029/1999GL011000.
Hsu, Y.J., Simons, M., Avouac, J.P., Galetzka, J., Sieh, K., Chlieh, M., Natawidjaja, D., Prawirodirdjo, L., Bock, Y., 2006. Frictional afterslip following the 2005 Nias–Simeulue earthquake, Sumatra. Science 312, 1921–1926.
Hsu, Y.J., Yu, S.B., Chen, H.Y., 2009. Coseismic and postseismic deformation associated with the 2003 Chengkung, Taiwan earthquake. Geophysical Journal International 176, 420–430.
Marone, C., Vidale, J.E., Ellsworth, W.L., 1995. Fault healing inferred from time dependent variations in source properties of repeating earthquakes. Geophysical Research Letters 22, http://dx.doi.org/10.1029/95GL03076.
Omori, F., 1894. On the aftershocks of earthquakes. Tokyo Imp. Coll. Sci. 7, 111–200.
Scholz, C.H., 1990. The Mechanics of Earthquakes and Faulting. Cambridge Univ., Press, New York.
Shcherbakov, R., Turcotte, D.L., 2004. A damage mechanics model for aftershocks. Pure and Applied Geophysics 161, 2379–2391.
Turcotte, D.L., Newman, W.I., Shcherbakov, R., 2003. Micro and macroscopic models of rock fracture. Geophysical Journal International 152, 718–728.
Utsu, T., 1961. A statistical study on the occurrence of aftershocks. Geophysical Magazine 30, 521–605.
Wang, J.H., 1994. On the correlation of observed Gutenberg–Richter's *b* value and the Omori's *p* value for aftershocks. Bulletin of the Seismological Society of America 84, 2008–2011.
Wang, J.H., 1995. Effect of seismic coupling on the scaling of seismicity. Geophysical Journal International 121, 475–488.
Wang, J.H., 1996. Velocity-weakening friction as a factor in controlling the frequency–magnitude relation of earthquakes. Bulletin of the Seismological Society of America 86, 701–713.
Wang, L., Wang, R., Roth, F., Enescu, B., Hainzl, S., Ergintav, S., 2009. Afterslip and viscoelastic relaxation following the 1999 *M* 7.4 İzmit earthquake from GPS measurements. Geophysical Journal International 178, 1220–1237.